Viscosity changes during crystallization of a shoshonitic magma: new insights on lava flow emplacement

Francesco VETERE[*], Hiroaki SATO[**], Hidemi ISHIBASHI[†,§], Rosanna DE ROSA[‡] and Paola DONATO[‡]

[*]*Institut für Mineralogie, Universität Hannover, Callinstr. 3, D-30167 Hannover, Germany*
[**]*Department of Earth and Planetary Sciences, Graduate School of Science, Kobe University,
Rokkodai 1-1, Nada-ku, 657-8501 Kobe, Japan*
[†]*Earthquake Research Institute, the University of Tokyo, Yayoi 1-1-1, Bunkyo-ku, Tokyo 113-0032, Japan*
[§]*Present address: Department of Geosciences, Faculty of Science, Shizuoka University,
Ohya 836, Suruga-ku, Shizuoka 422-8529, Japan*
[‡]*Dipartimento di Scienze Della Terra, Università della Calabria,
via P. Bucci I-87036 Arcavacata di Rende (CS), Italy*

Viscosity changes during the crystallization of a shoshonitic lava from the Vulcanello peninsula (Aeolian Islands, southern Tyrrhenian Sea, Italy) were measured by use of a electromagnetic rotational viscometer under Ni–NiO buffered conditions at temperatures ranging from 1539 K to 1381 K. Results showed an increase in effective viscosity from 131 Pa s to 15320 Pa s as the crystal content increased from 0 vol% to ~ 14 vol%. The crystallization processes in the nominally dry shoshonite began at 1420 K with the formation of clinopyroxene, which was followed by the formation of plagioclase and olivine at 1401 K. Experimental observations differed from predictions derived from the use of the Einstein-Roscoe equation with the Marsh (E-R-M) parameter at crystal contents higher than 8 vol%. The relative viscosity of samples was larger than that calculated by E-R-M by a factor of up to 9.5 as the temperature decreased to 1381 K. The large departure of the experimental results from the E-R-M equation predictions was likely caused by the interaction of elongated pyroxene crystals. The measured viscosity data were used to estimate the potential for emplacement of shoshonitic lavas.

Keywords: Viscosity, Concentric cylinders, Crystal morphology, Shoshonite, Vulcanello

INTRODUCTION

A detailed understanding of volcanic processes requires accurate experimental data regarding the chemical and physical properties of magmas. Among these properties, the rheological characteristics of magmas, including the viscosity of the liquid phase and the fraction and morphologies of crystals, are critically important to analyze. Viscosity is one of the most highly studied properties of silicate melts. Numerous viscosity models have been proposed and used not only to describe volcanic and other petrological processes, but also for industrial purposes such as in the production of glass.

Much effort has been put forth to quantify the effects of crystal content, crystal size, and crystal shapes on the viscosity of magma (Shaw, 1969; Murase and McBirney,

1973; Murase et al., 1985; Ryerson et al., 1988; Pinkerton and Stevenson, 1992; Lejeune and Richet, 1995; Pinkerton and Norton, 1995; Sato, 2005; Arbaret et al., 2007; Caricchi et al., 2007; Ishibashi and Sato, 2007; Costa et al., 2009). As described by Ishibashi (2009), one of the most frequently used equations to evaluate the relative viscosity (η_r) of a suspension is the Krieger-Dougherty (KD) equation (Krieger and Dougherty, 1959):

$$\eta_r = (1 - \Phi/\Phi_m)^{-v\Phi_m} \tag{1},$$

where Φ is the volume fraction of suspended particles; Φ_m, is the maximum packing density; and v, the intrinsic viscosity (or a measure of the crystal contribution to the viscosity of the suspension of the magmatic system). In this equation, $\eta_r = \eta_{eff}/\eta_m$ where η_{eff} is the effective viscosity of the suspension with a volume fraction ϕ of crystals and η_m is the viscosity of the melt.

The effective viscosity of crystal + melt systems is

F. Vetere, f.vetere@mineralogie.uni-hannover.de Corresponding author

often estimated with the Einstein-Roscoe (ER) equation (Einstein, 1906; Roscoe, 1952), assuming that $\nu \, \Phi_m = 2.5$:

$$\eta_{eff} = \eta_m \, (1 - \Phi/\Phi_m)^{-2.5} \qquad (2).$$

This equation is only valid if the shape of the particles can be approximated to be that of a sphere. According to Marsh (1981), a value of 0.6 for Φ_m is suitable to estimate the effects of crystals on the relative viscosity in magmatic systems, and this value corresponds to the crystal fraction at which a transition of the system to a rigid solid state will occur. However, it has been demonstrated that a value of $\Phi_m = 0.6$ is not always adequate for natural magmatic systems (Costa, 2005).

Recent studies on the viscosity of magmatic suspensions can be classified into three different categories according to the nature of the crystalline phases used in the experiments. One class of experiments uses crushed crystals such as quartz, alumina, and zircon as crystalline phases (Arbaret et al., 2007; Caricchi et al., 2007; Champallier et al., 2008, Vetere et al., 2010). These phases (crystals or analogous material) are often used because they have a low solubility in aluminosilicate melts. Hence, they are not expected to affect significantly the chemical composition of the melt. However, with this procedure the melt composition is expected to change as a function of temperature and this can cause problems for data interpretation (i.e., the composition of the silicate melt is not constant). When using this procedure, the crushed crystals may have angular edges that can lead to an increase in crystal-crystal interactions as compared to euhedral crystals that are polygonal in shape.

A second class of experiments used to study the viscosity of magmatic suspensions uses natural crystalline material. The magmatic suspension is directly heated to a desired temperature before its rheological behavior is examined (Caricchi et al., 2008; Cordonnier et al., 2009).

A third class of experiments uses natural rocks melted at extremely high temperatures ($\sim$ 1600 °C). Crystals are produced in these experiments during the crystallization process of the melt at subliquidus conditions. The rheological behavior of the crystal and melt suspension can be examined at a variety of different temperatures (Pinkerton and Norton, 1995; Sato, 2005; Ishibashi and Sato, 2007; Ishibashi, 2009; Vona et al., 2011). This third approach is advantageous because researchers can examine the sequential variation of both the crystal texture and rheological properties during the cooling of a sample. In the present study, we used this third type of approach to characterize the rheological properties of a shoshonitic lava from the Vulcanello peninsula (Aeolian Islands, southern Tyrrhenian Sea, Italy). The shoshonite had thin,

prismatic clinopyroxene crystals at the liquidus phase, which is different from previous experiments in which either tabular plagioclase or equigranular olivine were observed at the liquidus phase (Ishibashi and Sato, 2007; Ishibashi, 2009; Vona et al., 2011).

STARTING MATERIAL

The starting material was a natural shoshonite from the Vulcanello peninsula on Vulcano Island (the southernmost island of the Aeolian Archipelago, southern Tyrrhenian Sea, Italy) (Fig. 1). The Vulcanello peninsula is a lava platform with three nested scoria cones aligned NE–SW along the northern ring fault of the La Fossa caldera (Ventura et al., 1999; Blanco-Montenegro et al., 2007). Building of the Vulcanello peninsula started in 1000 A.D. with the formation of the first cone and ended in 1650 A.D. with the emplacement of the latitic lava flow on Punta del Roveto (Arrighi et al., 2006). According to Davì et al. (2009), the shoshonites of Vulcanello represent a slightly evolved product of a basaltic shoshonitic magma similar to that feeding the young (post 15 ka) Vulcano activity (Gioncada et al., 1998). According to Zanon et al. (2003) and Peccerillo et al. (2006), the basaltic shoshonitic magma chamber is settled within the continental lower crust at a depth of about 20 km. From this depth, the magma rose rapidly to the surface with a velocity of between 0.27 m s^{-1} and 3.2 m s^{-1} corresponding to an ascent time of between roughly 2 and 21 h (Vetere et al., 2007).

For the viscosity study, we used a lava sample representative of the shoshonites from the platform (VLO 8 in Davì et al., 2009). The rock had a porphyritic texture (modal abundance of phenocrysts is $\sim$ 20 vol%) with phenocrysts up to 2 mm in size settled in a microcrystalline groundmass. The most abundant phase of the phenocryst was clinopyroxene ($Wo_{46}En_{39}Fs_{15}$–$Wo_{42}En_{51}Fs_7$) whose modal abundance was $\sim$ 13 vol%. Also abundant were feldspars (both plagioclase and alkali-feldspar, $\sim$ 5 vol%) and olivine (Fo_{47-78}–Fa_{22-53}) (Fig. 5). Phenocrysts and microphenocrysts of leucite and iron-titanium oxides were also present. The groundmass was primarily composed of feldspars and leucite, while mafic phases (clinopyroxene, olivine, and Ti-magnetite) were present but less abundant. Feldspars occurring in the groundmass had compositions similar to those of the phenocrysts ($An_{55-63}Ab_{39-44}Or_{6-50}$). The bulk rock chemical composition of the sample is reported in Table 1. It was characterized by 53.7 wt% SiO_2 and the total alkalis were 9.66 wt%. The K_2O/Na_2O ratio was $\sim$ 1.2.
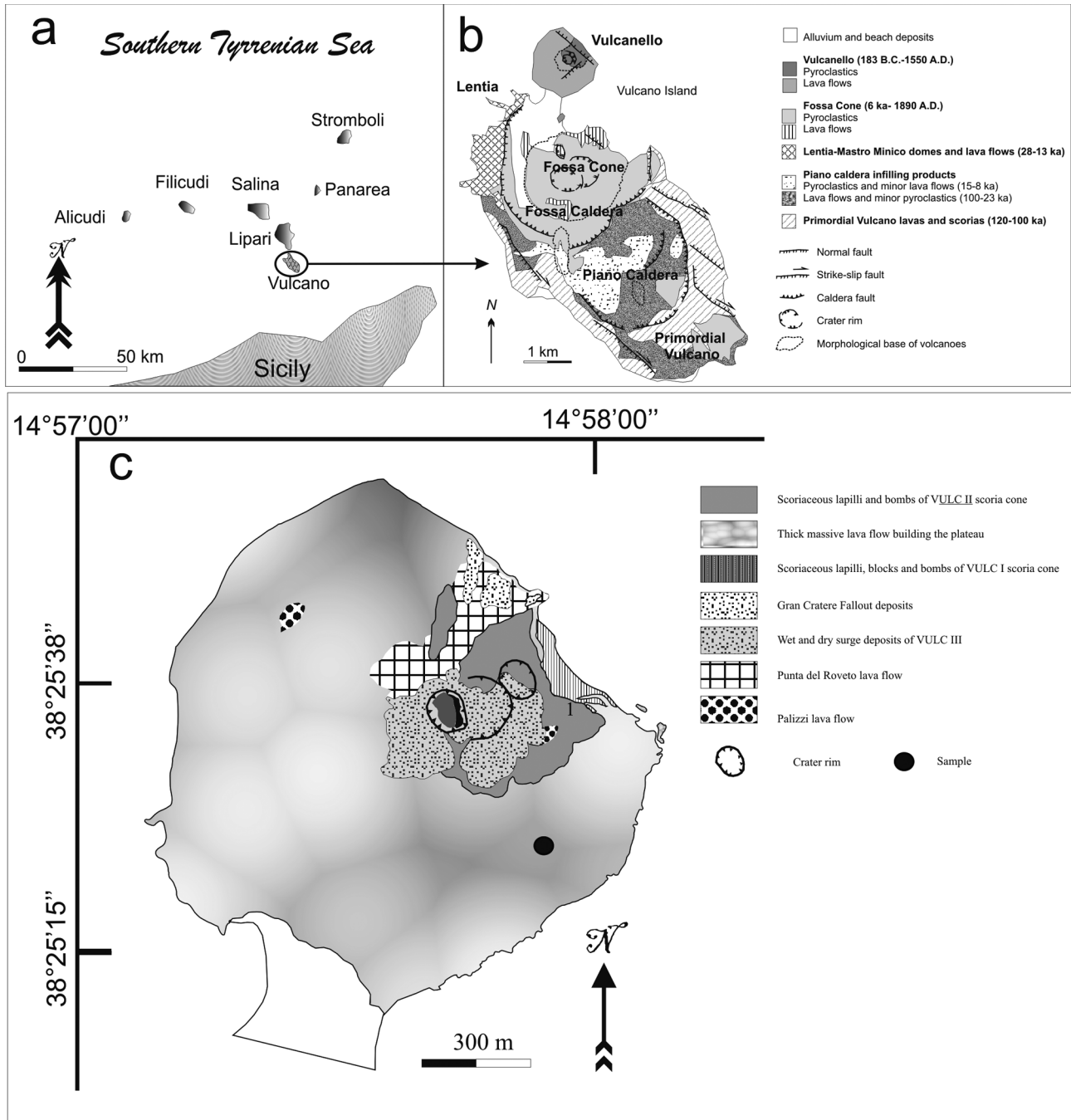
Figure 1. (a) Southern Tyrrhenian Sea sketch map. (b) A geological map of Vulcano Island (modified from Vetere et al., 2007). (c) A geological map of Vulcanello (modified from De Astis et al., 2006). The black circle indicates where samples were collected.

EXPERIMENTAL EQUIPMENT AND MEASUREMENTS

The techniques used to determine viscosity and to sample the experimental products at various stages in this experiment were identical to those described by Sato (2005) and Ishibashi and Sato (2007). We measured viscosity by use of an electromagnetic rotational viscometer (TV-10U,

Toki Sangyo Co. Ltd., Japan). The concentric cylinder apparatus used in the rotational viscometer enabled viscosity measurements of suspensions in the low viscosity range (e.g., Spera et al., 1988). As sample holder we used an Fe-bearing Pt crucible (30 mm inner diameter and 60 mm in height). The samples were crushed (particles size <2 mm) and repeatedly fused in crucibles for more than 10 hours at 1600 K. Redox conditions within the furnace

Table 1. Electron microprobe analyses of the bulk rock, glasses, and crystals after the viscosity experiments[†]

T (K)	No.	SiO$_2$	TiO$_2$	Al$_2$O$_3$	FeO[§]	MnO	MgO	CaO	Na$_2$O	K$_2$O	P$_2$O$_5$	Total	#Mg	#Ca	Comment
		53.66	0.63	17.27	7.80	0.15	3.39	6.74	4.43	5.23	0.42	100.01	0.437	0.457	VLO 8*
1539	14	54.03	0.66	15.72	8.22	0.14	3.90	7.18	3.42	5.10	0.42	98.83	0.458	0.537	Melt
		0.28	0.03	0.41	0.19	0.02	0.24	0.31	0.11	0.18	0.02	0.45			Std
1509	11	54.06	0.65	16.04	8.11	0.14	3.83	7.14	3.44	5.15	0.42	98.98	0.457	0.534	Melt
		0.12	0.02	0.28	0.14	0.03	0.11	0.16	0.18	0.14	0.02	0.33			Std
1479	15	53.91	0.64	15.98	8.22	0.14	3.9	7.22	3.4	5.12	0.41	98.94	0.458	0.54	Melt
		0.39	0.03	0.43	0.30	0.02	0.14	0.27	0.14	0.19	0.02	0.37			Std
1459	15	53.62	0.65	15.54	8.46	0.15	4.06	7.30	3.41	5.03	0.41	98.64	0.461	0.541	Melt
		0.35	0.03	0.16	0.11	0.02	0.09	0.14	0.12	0.08	0.03	0.39			Std
1439	11	53.97	0.64	15.73	8.46	0.15	4.08	7.39	3.39	4.98	0.4	99.18	0.463	0.546	Melt
		0.20	0.01	0.14	0.16	0.03	0.08	0.16	0.12	0.07	0.02	0.26			Std
1420	12	54.17	0.65	15.79	8.51	0.15	3.93	7.22	3.49	5.12	0.41	99.43	0.451	0.534	Melt
		0.41	0.02	0.3	0.17	0.03	0.22	0.27	0.11	0.09	0.02	0.48			Std
	61	51.3	0.6	3.92	7.66	0.17	15.37	21.12	0.3	0.06	-	100.51	0.781	0.975	Cpx
		0.66	0.10	0.55	0.22	0.03	0.51	0.33	0.06	0.02	-	0.49			Std
1410	22	53.97	0.65	16.14	8.54	0.15	3.57	6.66	3.55	5.23	0.43	98.9	0.427	0.509	Melt
		0.27	0.02	0.12	0.12	0.02	0.07	0.10	0.16	0.07	0.02	0.28			Std
	80	50.76	0.65	4.16	7.94	0.17	15.07	21.22	0.29	0.04	-	100.31	0.772	0.976	Cpx
		0.89	0.15	0.77	0.38	0.03	0.69	0.38	0.05	0.02	-	0.51			Std
1401	19	53.97	0.64	16.47	8.65	0.14	3.10	6.18	3.66	5.44	0.44	98.69	0.39	0.483	Melt
		0.25	0.03	0.20	0.13	0.02	0.11	0.16	0.14	0.09	0.02	0.38			Std
	8	39.24	0.02	0.05	23.11	0.46	40.71	0.39	0.01	0.02	-	104	0.758	0.943	Ol
		0.37	0.02	0.01	0.41	0.02	0.35	0.02	0.02	0.01	-	0.4			Std
	90	50.77	0.62	4.11	8.09	0.18	14.96	21.38	0.3	0.03	-	100.45	0.767	0.976	Cpx
		0.79	0.11	0.64	0.40	0.02	0.64	0.31	0.05	0.01	-	0.48			Std
	1	53.16	0.05	27.75	1.17	0.00	0.20	11.88	3.24	1.02	-	98.47	0.237	0.67	Plg
1391	28	53.97	0.66	16.67	8.65	0.15	2.84	5.81	3.74	5.59	0.47	98.56	0.369	0.462	Melt
		0.29	0.03	0.16	0.13	0.02	0.09	0.14	0.11	0.1	0.02	0.45			Std
	15	38.91	0.01	0.04	24.42	0.48	39.62	0.41	0.02	0.01	-	103.93	0.743	0.919	Ol
		0.22	0.01	0.01	0.54	0.02	0.46	0.03	0.02	0.01	-	0.5			Std
	91	50.71	0.59	4.03	8.09	0.18	15.08	21.49	0.3	0.04	-	100.5	0.769	0.976	Cpx
		0.84	0.12	0.72	0.44	0.03	0.61	0.26	0.05	0.02	-	0.54			Std
	5	53.76	0.05	27.49	1.04	0.02	0.13	11.31	3.49	1.13	-	98.42	0.186	0.642	Plg
		0.43	0.02	0.20	0.11	0.01	0.04	0.18	0.10	0.05	-	0.52			Std
1381	15	54.43	0.69	16.65	8.86	0.16	2.56	5.48	3.87	5.79	0.50	98.99	0.34	0.439	Melt
		0.23	0.02	0.11	0.13	0.02	0.12	0.1	0.07	0.12	0.02	0.32			Std
	27	38.77	0.01	0.04	27.06	0.54	38.04	0.39	0.02	0.02	-	104.88	0.715	0.918	Ol
		0.27	0.01	0.01	0.58	0.02	0.58	0.03	0.02	0.01	-	0.44			Std
	64	50.92	0.61	4.11	8.12	0.17	15.07	21.48	0.31	0.03	-	100.83	0.768	0.974	Cpx
		0.86	0.1	0.61	0.42	0.02	0.6	0.3	0.04	0.01	-	0.46			Std
	3	0.3	4.56	6.44	84.72	0.26	4.5	0.2	0.02	0.08	-	101.08	0.087	0.844	Mt
		0.06	0.04	0.09	0.09	0.01	0.02	0.07	0.02	0.02	-	0.05			Std
	21	54.05	0.04	27.47	1.08	0.01	0.10	11.07	3.67	1.17	-	98.65	0.143	0.625	Plg
		0.36	0.02	0.21	0.08	0.01	0.01	0.28	0.16	0.07	-	0.32			Std

[†] Abundances expressed as wt%.

[§] Total iron is given as FeO. * From (Davì et al., 2009). Std refers to the standard deviation. Cpx, Plg, Ol and Mt to clinopyroxene, plagioclase, olivine, and magnetite, respectively.

were controlled by use of a H$_2$ and CO$_2$ gas mixture. The experimental oxygen fugacity corresponded to that of the Ni–NiO buffer at various experimental temperatures (Huebner, 1982). A starting depth of ~ 50 mm was selected for the placement of alumina rod to expel any vesicles present. At each experimental temperature, the tip of an alumina rod (6 mm in outer diameter) was placed just above the crucible for several minutes to allow for thermal equilibration subsequent to its immersion in the sample. Ultimately, we set the end of the ceramic rods to just 2 mm above the bottom of the crucible. The presence of crystals during viscosity measurements can lead to a monotonous decrease of the apparent viscosity over time (i.e., thixotropic behavior). To avoid this inconvenience, we initially increased and then decreased the rotational rate of the apparatus in a step-wise manner. After the

maximum rotational rate was attained, the viscosity and torque data were mostly constant and these data were used in this study.

The principles of concentric cylinder rotational viscometry are described in detail by Ishibashi (2009) and only the essential points are reported here.

One of the simplest models suitable for describing the rheology of magma is the power law fluid model:

$$\tau = m\varepsilon^n \qquad (3),$$

where τ is the shear stress; ε is the shear strain rate; and m and n are constants. Note that the parameter m corresponds to viscosity at $\varepsilon = 1$ s^{-1}. If a sample behaves as power law fluid, the relationship between the rotational angular velocity, Ω, and shear stress on the surface of the inner cylinder, τ_i, is described as follows (Ishibashi, 2009):

$$ln\tau_i = nln\Omega + lnm - nln[n(1 - k^{1/n})/2] \qquad (4),$$

where k is (R_i^2/R_c^2), and R_i and R_c are radii of the inner and outer cylinders, respectively. Using equation (4), we can simultaneously obtain values of both m and n from the τ_i –Ω dataset. When $n = 1$, equation (4) is reduced to the following:

$$\tau_i = 2m\Omega(1 - k)^{-1} \qquad (5).$$

This equation is identical to the basic equation of concentric cylinder viscometry for Newtonian fluids (e.g., Shaw, 1969; Landau and Lifschitz, 1970), indicating that equation (4) can also be applied to a Newtonian fluid. It is possible to check whether a sample (or fluid) can be approximated as power law fluid (including Newtonian fluid) or not by examining the relationship between $ln(\tau_i/\Omega)$ and $ln\Omega$. When a fluid behaves as a power law fluid or a Newtonian fluid, $ln(\tau_i/\Omega)$ correlates linearly with $ln\Omega$, and $ln(\tau_i/\Omega)$ is constant with changing $ln\Omega$.

A standard oil JS160000 was used to calibrate the system and to correct for the end-effect of the rod. This oil had a viscosity of ~ 148 Pa s at 293.15 K and showed Newtonian behavior (details are given in Ishibashi, 2009).

Figure 2 shows the temperature and time schedule of the experiments. Experiments were performed with temperatures ranging from 1539 K to 1381 K. The starting material was kept at 1539 K for more than 48 hours to ensure a homogeneous molten rock. The glass composition of the experiments is reported in Table 1. At 1539 K, 1479 K, 1439 K, and 1401 K, a type B thermocouple was inserted into the ceramic rod to calibrate the temperatures of the crucible in the furnace. The temperatures within the
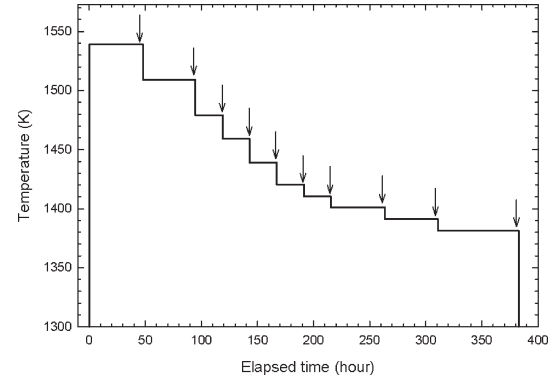

Figure 2. Sampling times and temperatures used in this study. The arrows indicate when viscosity measurements were taken and when samples were collected.

crucibles were mostly uniform (within 1 K) horizontally, and varied less than 10 K vertically. After viscosity measurements were taken and temperature calibrations were performed, alumina rods were pulled out of the samples, quenched in air, and polished thin sections of the rods were prepared for microprobe analyses. Microprobe analyses were used to determine the composition of the melt (glass) and crystal content and to view textural details. It is also important to note here that the samples were molded from their tips to their upper ends so that we could examine vertical variations in the textures of the shoshonite. The attached samples were usually less than 1 mm thick around the rods, and we prepared both normal cross sections and sections tangential to the elongated rods. Subsequently, temperatures were lowered and the sampling procedures were repeated. For each experimental temperature, a new alumina rod was used to avoid any possible contamination from previous steps. Ten viscosity measurements were performed over an interval of time covering more than 380 h. Figure 2 shows that each sequence of viscosity measurements and cooling lasted at least 20 h. To ensure equilibrium phase relations, the time interval before each measurement was taken at lower temperatures was increased to about 2–3 days. However, as reported by Ishibashi and Sato (2007), 20 h should be enough time to ensure equilibrium phase relationships in basaltic systems when this type of viscosity measurement technique is used.

The height (or depth) of the liquid in the crucible decreased from an initial value of 47.1 mm to 25.3 mm by the end of the measurements as a result of losses from repeated sampling. The depth of the liquid was obtained by measurements of the solid surface of the sample in the crucible before and after the experiment, taking into consideration the effect of the insertion of the rod and the expansion of volume due to high temperatures and melting.

The interpolated depth of the liquid during measurements at each temperature was consistent with the observed height of the liquid surface at the time of first contact of the end of the rod with the silicate melt during the insertion.

RESULTS AND DISCUSSION

Phase chemistry

An electron microprobe (JEOL JXA8900) with a wavelength dispersive spectrometer (WDS) was used to analyze the composition of samples after viscosity measurements were taken. These analyses were conducted at the Venture Business Laboratory, Kobe University, Japan.
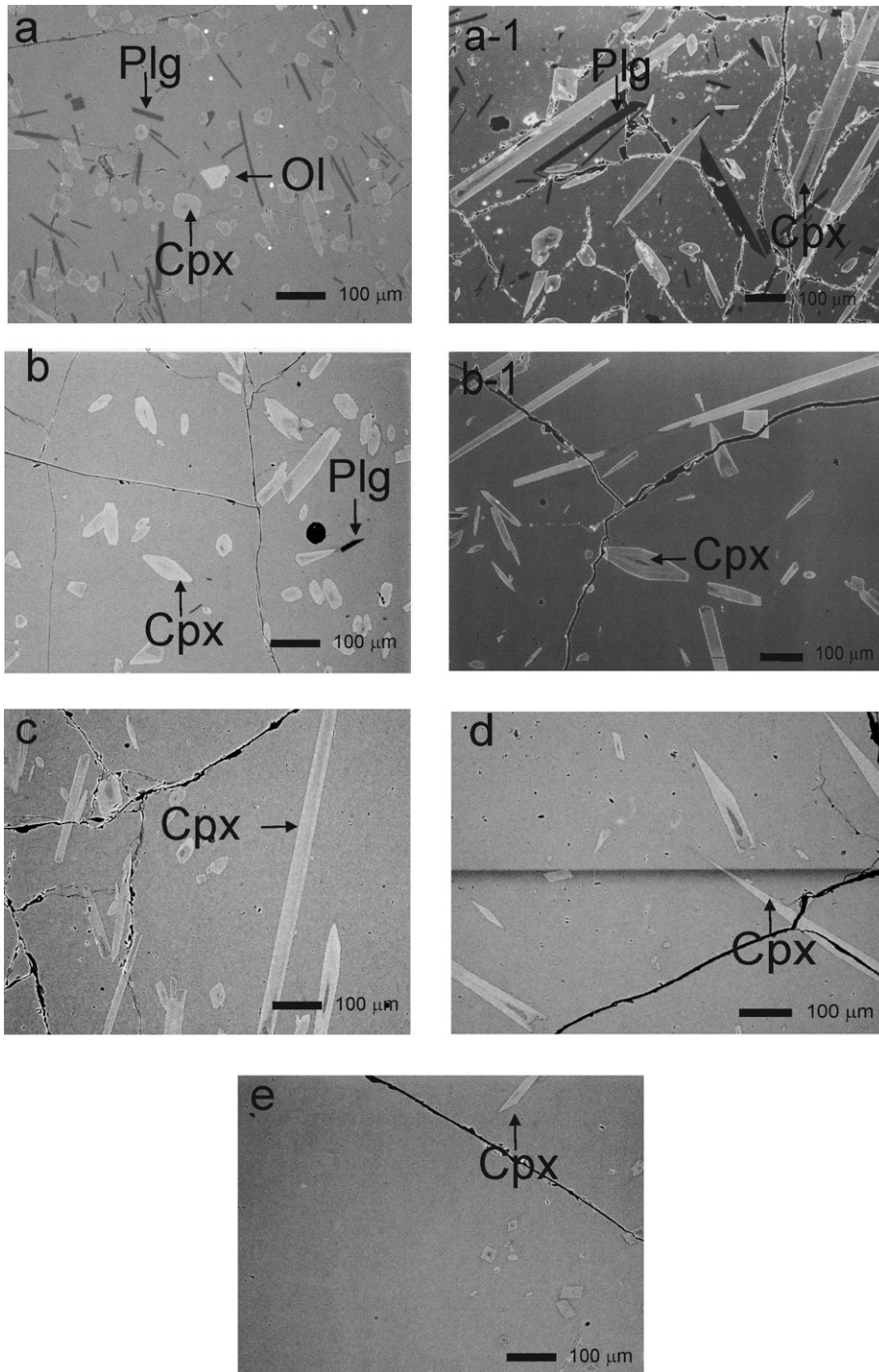

Figure 3. Back-scattered electron (BSE) images of crystal-bearing shoshonite glasses containing clinopyroxene (Cpx), plagioclase (Plg), and olivine (Ol) crystals. Images (a), (b), (c), (d), and (e) are cross sections of samples cut normally to the elongation of the alumina sampling rods that were collected at 1381 K, 1391 K, 1401 K, 1410 K, and 1420 K, respectively., Images (a-1) and (b-1) represent rod-parallel sections collected at 1381 K and 1391 K, respectively.
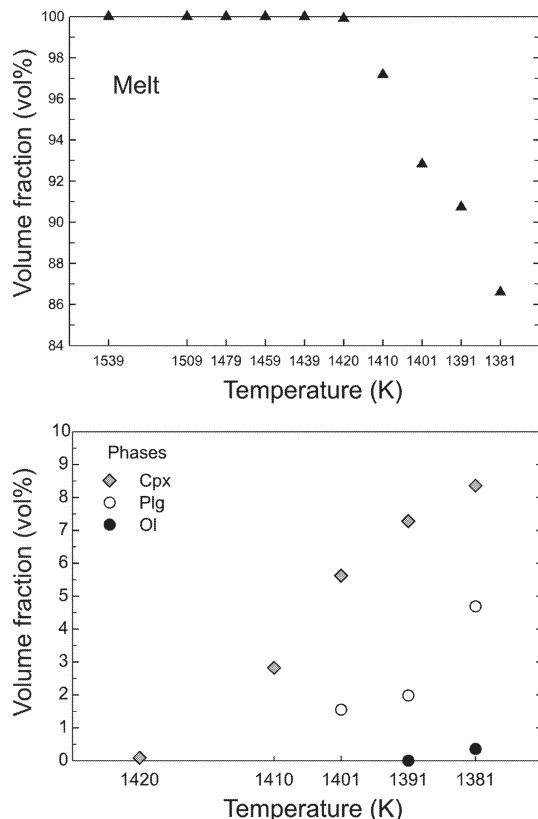
Figure 4. Temperature induced changes in the volume of melt and crystal content. Crystals are clinopyroxene (Cpx), plagioclase (Plg), and olivine (Ol).
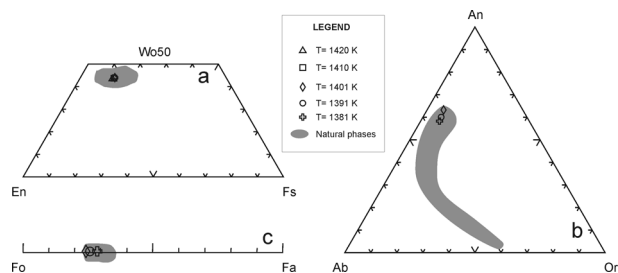

Figure 5. Phase composition of the experimental products and of the natural sample. Graphs represent the phase composition of (a) pyroxene, (b) feldspar, and (c) olivine. Natural phase compositional fields are shown in gray for comparative purposes.

Analytical conditions were: 12 nA, 15 KV accelerating voltage, and 20 s counting time with 10 s counting on both sides of the peak for background except for Na analyses of glass for which broad beam, 4 s counting and 2 s background were performed without a peak search.

From 1539 K to 1439 K, only the melt phase was detected (Table 1). Figure 3 shows back-scattered electron images (BSE) of the run products for samples in which crystals occurred. Starting from 1420 K, clinopy-

roxene crystallized followed by plagioclase and olivine at 1401 K (Table 1 and Figs. 3, 4). Clinopyroxene has an augitic composition that remains nearly constant with decreasing temperatures, and it is similar to that of the natural rock. Plagioclase can be classified as labradorite whereas the composition of olivine is Fo_{71-75}. The composition of both phases matched that found in the natural sample. The phase compositions are reported in Table 1 and Figure 5.

The volume fraction of the crystals was evaluated by the mass balance calculation used by Le Maitre (1979), and it varied between 0.1 vol% at 1420 K and 13.5 vol% at 1381 K (Table 2). The amount of clinopyroxene in the samples increased progressively from 1 vol% to 8.4 vol% when temperatures decreased from 1420 K to 1381 K (Table 2 and Fig. 4). The maximum value of clinopyroxene in the samples was in agreement with levels found in other studies of natural lava samples collected from the Vulcanello platform. In other studies, clinopyroxene phenocryst contents ranged from 7.6 vol% to 13 vol% (Davì et al., 2009).

The volume of melt decreased progressively from 100% to 86.5% with decreasing temperatures (Fig. 4). The maximum decrease of ~ 5% was observed between

Table 2. Experimental conditions and results of viscosity experiments, crystals content by mass balance and image analyses approach

| T | melt | Plg crystals | Ol crystals | Cpx crystals | crystals (tot.) | crystals (tot.) | η |
| | by mass balance | by mass balance | by mass balance | by mass balance | by mass balance | by image analysis | This work |
(K)	(vol%)	(vol%)	(vol%)	(vol%)	(vol%)	(vol%)	(Pa·s)
1539	100.00	0.00	0.00	0.00	0.00	0.00	130.8±3.2
1509	100.00	0.00	0.00	0.00	0.00	0.00	168.6±1.0
1479	100.00	0.00	0.00	0.00	0.00	0.00	239.9±4.7
1459	100.00	0.00	0.00	0.00	0.00	0.00	315.7±2.4
1439	100.00	0.00	0.00	0.00	0.00	0.00	563.0±1.8
1420	99.90	0.00	0.00	0.10	0.10	0.89±0.3	900.6±54.4
1410	97.20	0.00	0.00	2.80	2.80	4.08±0.9	2555.2±181.4
1401	92.90	1.50	0.00	5.60	7.10	9.02±1.8	4591.1±179.8
1391	90.70	2.00	0.00	7.30	9.30	11.28±2.3	8201.2±145.3
1381	86.50	4.70	0.40	8.40	13.50	14.37±2.5	15320.5±531.9

Note: η refers to viscosity.
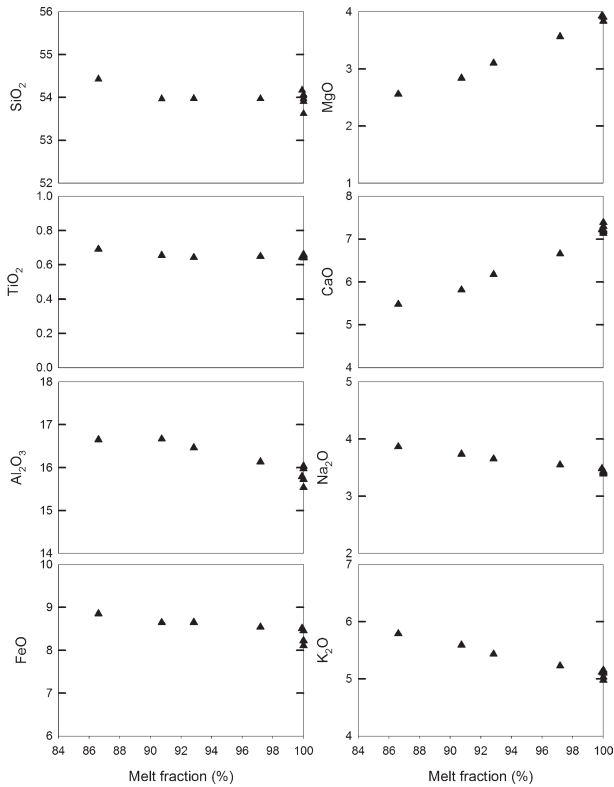
Figure 6. Relationship between the fraction of the melt and the concentration of major elements in the melt.

1410 K and 1401 K. The SiO_2 content of the residual glass was fairly constant for all of the temperatures except for the lowest temperature range (e.g., melt fraction = 86.5%) where a slight increase in SiO_2 content was observed (Fig. 6). The MgO and CaO content decreased progressively from ~ 4.0 wt% to 2.5 wt% and from 7.3 wt% to 5.5 wt%, respectively. As the crystallization process proceeded, an increase of Al_2O_3, $FeO_{tot.}$, Na_2O, and K_2O was observed. The TiO_2 content remained almost constant (Fig. 6 and Table 1).

Image analyses of the run products

Back-scattered electron (BSE) images from crystal-bearing shoshonitic samples were collected after viscosity measurements were taken to obtain information about the volume fraction and the shape distribution of the crystals. Image analysis was performed to extract and characterize the crystal shapes from the gray-scale slides. To identify the crystals to be analyzed, it was necessary to transform the original 256 gray level images into binary ones (Dellino and La Volpe, 1996; Loncaric, 1998). For each crystal, the following two shape parameters were determined (Cox and Budhu, 2008):

Aspect ratio (AS) = major axis/minor axis   (6),

Form factor (FF)
= [4π (2D surface area)]/(perimeter^2)   (7).

The aspect ratio and form factor yield information about the degree to which 2D particles are elongated and the extent of their surface irregularities (roughness), respectively. A circle, which represents a perfectly rounded particle, has an AS = FF = 1. As the irregularity of the particle shape increases, the form factor decreases. We used ImageJ, 1.37v software (Wayne Rasband, National Institutes of Health, USA) (available at http://rsbweb.nih.gov/ij to perform the image analyses. Two or three images of approximately 700 × 1000 μm in size and with a resolution of 1200 dpi were analyzed for each sample. The image analyses were performed on both vertical and horizontal sections. The number of crystals counted in each image varied from 15 to 866. The volume of crystals derived by the use of mass balance equations was compared to estimates obtained by image analyses. The crystal volumes obtained by ImageJ software were slightly higher with respect to the values obtained via the use of mass balance equations (Table 2). It should be noted that the applied image analysis methodology only provides average values. Furthermore, we did not test for possible lateral textural heterogeneities or changes in crystal alignment along the entire crucible radius. Therefore, we cannot exclude the possibility that the system may have been disturbed during the retraction of the ceramic rod, which could have caused some crystal realignment.

Figure 7 summarizes the distribution of the shape parameters of the crystals from the different experimental runs. The distributions of the aspect ratio and form factor were similar in the different experimental runs. The calculated form factor values indicate that the shape of the crystals is similar to that observed in magmatic rocks (e.g., Iezzi and Ventura, 2002). Half of the crystals, 50.5%, had an AS <3 and the other half of the total, 49.5%, had an AS ≥3. These data are for 2D sections, and the apparent aspect ratios may not correspond to aspect ratios obtained from 3D sections.

The shape distributions of the crystals in the different experimental runs were comparable, elongated, and acicular (Fig. 3). These shapes are expected to influence the viscosity of the suspension as this has already been demonstrated in previous studies (Ishibashi, 2009 and references therein). Moreover, a comparison was done between the aspect ratios and form factors of clinopyroxene and plagioclase for experiments run at 1381 K. As shown in Figure 8, both the aspect ratios and form factors of clinopyroxene and plagioclase were comparable. The form factors for plagioclase were lower than the values found for clinopyroxene, and were reflective of the higher

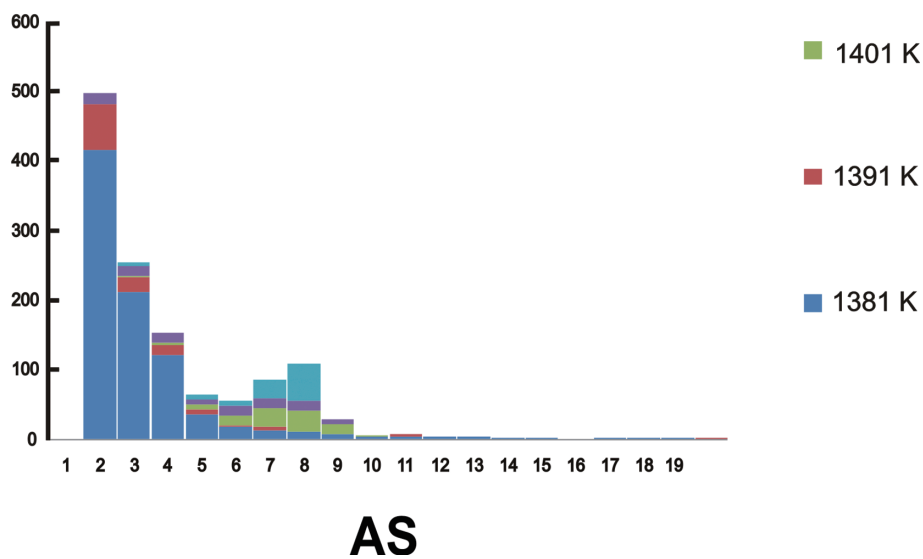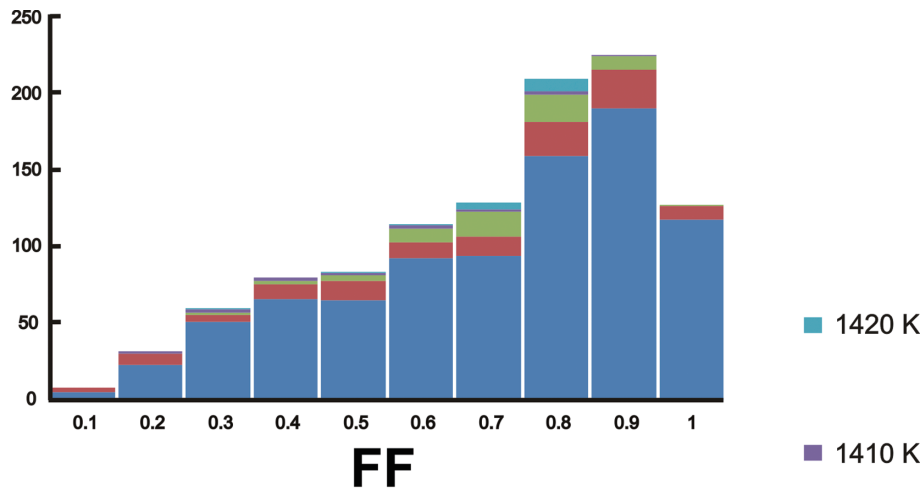**Figure 7.** Distribution of the aspect ratio (AS) and the form factor (FF) for crystals contained in the experimental products. Data are based on two to three back-scattered electron (BSE) images for each experiment.
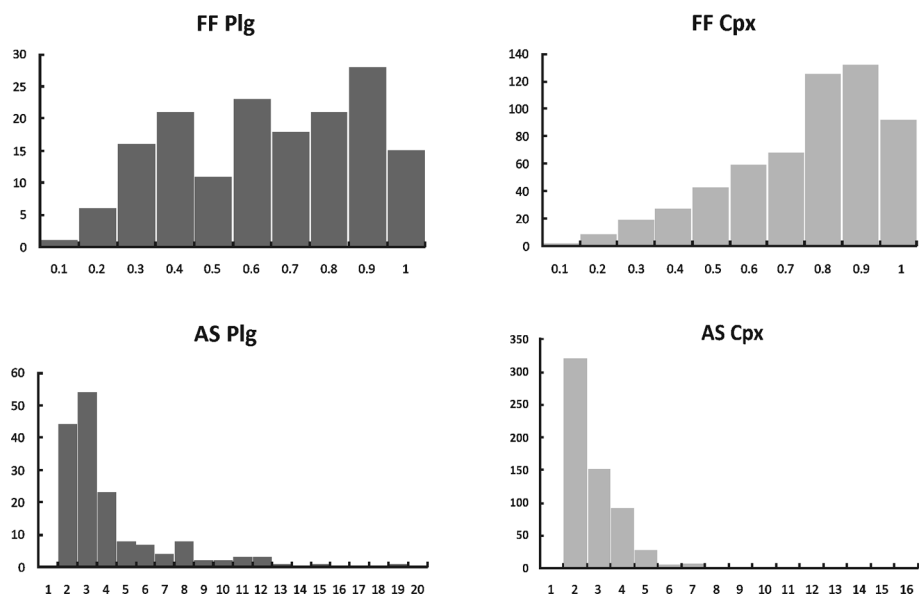

Figure 8. Distribution of the aspect ratio (AS) and the form factor (FF) for plagioclase (Plg) and clinopyroxene (Cpx) crystals in the experimental run products at 1381 K.
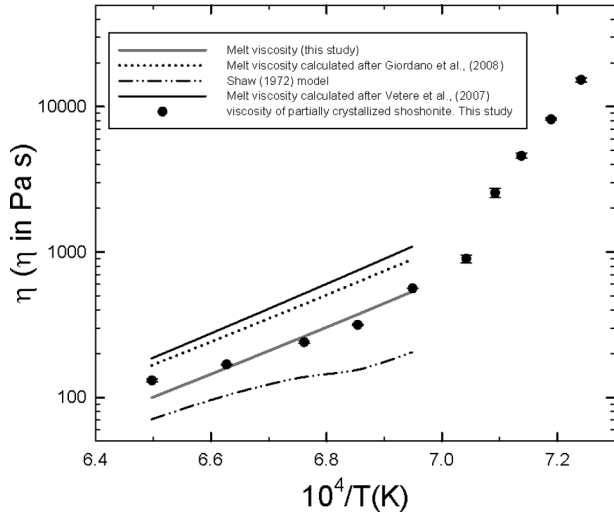
amounts of irregularity found for plagioclase crystals.

Textural analyses of the run products

Higgins (2000) pointed out that for a massive rock (no preferential orientation of the crystals) and crystals modeled as parallelepipeds, the mode of the *w/l* is equal to S/I, where the *w/l* and S/I denote the width/length and short to intermediate dimension, respectively. The ratio *I/L* (*L* = long dimension) can be estimated from the skewness of the *w/l* distribution as follows:

Skewness
= (mean *w/l* − mode *w/l*)/standard deviation *w/l*,
and *I/L* = Skewness + 0.5 (8).

By use of these relationships, we estimated the morphological parameters of clinopyroxene and plagioclase in all of the run products. We performed image analyses on 536 clinopyroxene and 68 plagioclase crystals. The average S/I/L ratio is 0.11:0.16:1 for clinopyroxene and 0.14:0.94:1 for plagioclase. Therefore, clinopyroxene crystallizes with an elongated, prismatic morphology, while plagioclase crystallizes with a thin, tabular morphology. Although the obtained morphological parameters may include errors due to the partial preferred orientation of crystals in the run products, these estimated crystal morphologies may be relevant to the evaluation of relative viscosity in the presence of crystals.

Viscosity measurements and comparison with models

Each point shown in Figure 9 is the result of viscosity measurements taken during the latter half of the measurements where we decreased the rotation rate in a step-wise manner. This procedure was performed for each temperature step in order to determine the viscosity of partially crystallized shoshonite (Table 2). In Figure 9, $ln(\tau/\Omega)$ was plotted versus $ln\Omega$. Linear relationships were observed between $ln(\tau/\Omega)$ and $ln\Omega$ for each run temperature, indicating that our assumption that the material would behave like a power law fluid was valid. By use of equation (4), parameters *m* and *n* were determined for each run temperature (for details refer to Ishibashi, 2009). The values obtained for *m* and *n* are listed in Table 3. The results show

Figure 9. Ln (τ/Ω) ratios plotted against $ln\Omega$ at different temperatures. Black lines are power law regression lines. Regression parameters are shown in Table 3.

that the values obtained for parameter *n* were slightly lower than 1 at run temperatures of 1420, 1410, 1401, and 1381 K. However, most of these *n* values were larger than 0.95, and were indicative of a very weak shear thinning behavior. Therefore, under these experimental conditions the samples can be approximated to be Newtonian fluids. Even for the smallest *n* value of 0.934 observed at 1410 K, the ratio of viscosity to *m* varied only in the range of 0.74-1.36 with ±2 orders of magnitude variation of ε.

As temperatures decreased from 1539 K to 1381 K, the value of *m*, or viscosity at ε = 1 s^{-1}, continuously increased from 134 Pa s to 12687 Pa s (Table 3). We compared our results on the viscosity of pure melts to modeled values obtained from Vetere et al. (2007) (model built using viscosity data derived from the same composition used for this study), and those from Shaw (1972) and Giordano et al. (2008) (general viscosity models) (Fig. 10). Our experimental data fell between the calculated viscosities of Shaw (1972) and those of Giordano et al. (2008) and Vetere et al. (2007). Shaw's model assumed Arrhenian temperature dependence whereas those of Giordano et al. (2008) and Vetere et al. (2007) assumed non-Arrhenian temperature dependence. These differences can be partially explained by considering the role of oxygen fugacity in our experiments. Data presented in the literature (Dingwell and Virgo, 1988; Mysen and Virgo, 1989; Dingwell, 1991; Liebske et al., 2003; Vetere et al.,

Table 3. Power law fluid parameters, *m* and *n*, for all run temperatures

T(K)	1539	1509	1479	1459	1439	1420	1410	1401	1391	1381
m	134	168	239	309	392	737	1784	4069	7740	12687
n	1.023	1.006	1.005	1.002	0.991	0.954	0.934	0.978	0.995	0.963
R^2	0.9999	0.9999	0.9999	0.9999	0.9999	0.9999	0.9999	0.9999	0.9999	0.9999

Figure 10. Comparison of the observed shoshonite effective viscosities with the viscosity of crystal-free melts (gray line) extrapolated by use of a simple equation that was based upon a crystal-free melt viscosity of $ln\ \eta$ (Pa s) = −7.09036 + 27695556/T^2. Also shown are melt viscosities calculated with the models described in Vetere et al. (2007) (black solid line), Giordano et al. (2008) (dotted line), and Shaw (1972) (dash dot line).

2008) have shown that the oxidation state of Fe is an important parameter that needs to be taken into account when modeling the viscosity of silicate melts with relatively high Fe contents. The viscosity of the melt in the system Na–Si–Fe–O composition NS4F40 at 1473 K described by Dingwell and Virgo (1988), decreased by 0.81 log units when the Fe^{2+}/Fe_{tot} ratio increased from 0 to 0.77. Moreover, a decrease in viscosity of 0.34 log units was found for a $NaFeSi_2O_6$ melt at 1703 K when the Fe^{2+}/Fe_{tot} ratio increased from 0.08 to 0.82. As shown by Liebske et al. (2003), as the Fe^{2+}/Fe_{tot} ratio increases from 0.42 to 0.79 in an andesitic melt at 1061 K, the viscosity will decrease by ∼ 1.7 log units. The model results reported in Figure 10 do not take the experimental reducing conditions into account, which can lead to underestimates or overestimates of the melt viscosity.

If we extrapolate the melt viscosity to 1381 K, the difference between melt viscosity and a partially crystallized shoshonite with a crystal content of ∼ 14 vol%

would be about 12000 Pa s. The experimental data begin to depart from the literature modelsat 1401 K and a crystal content of ∼ 8 vol%.

In regards to partially crystallized systems (e.g., silicates, ceramics, or other industrial products), there are a number of recent studies that analyzed the effect of crystals on the rheological properties of 'magmas' by adopting experimental techniques that were alternative to the ones used here. These studies produced highly accurate results. Caricchi et al. (2007) performed creep experiments on haplogranitic melts containing 2.7 wt% of dissolved water and various amounts of crushed quartz crystals by use of a Paterson-type apparatus. At temperatures ranging 773-1173 K and a confining pressure of 250 MPa, they observed Newtonian behavior of the system for strain rates lower than 10^{-5} s^{-1}, and independent from the volume of crystals. Above this threshold, an increase of strain rate always induced a decrease of viscosity (shear thinning). In our experiments, probably due to the relatively low amount of crystals (resulting in a very weak shear thinning behavior), results were indicative of Newtonian fluid behavior. Comparing our results with the Caricchi et al. (2007) model, it must be noted that in any type of rotational viscometer the shear strain rate varies along the radial direction of rotation. Therefore, it is difficult to determine a unique value of shear strain rate for each measurement. However, our method enables direct determination of flow parameters (i.e., the parameters m and n in the power law fluid model can be determined). From m and n, we can determine apparent viscosity at an arbitrary shear strain rate as:

$$\log \eta = \log m + (n-1) \log \varepsilon \qquad (9).$$

The apparent viscosity calculated by equation (9) was compared with viscosities calculated by the Caricchi et al. (2007) model at arbitrary shear strain rates. Using different shear rate values of 10^{-2}, 1, and 10 s^{-1}, the results show that the Caricchi et al. (2007) model is inappropriate for predicting the viscosity of partially crystallized shoshonite, at least in dilute and semi-dilute field ranges (0 < $\Phi \leq 0.25$ vol%) when parameter B (the intrinsic viscosity,

Table 4. Viscosity of melt and relative viscosity

T(K)	1539	1509	1479	1459	1439	1420	1410	1401	1391	1381
η_m [$]	149	103	207	361	583	855	1023	1189	1389	1605
η_r	0.88	1.64	1.16	0.87	0.97	1.05	2.50	3.86	5.91	9.54
η_r(ER)	1.00	1.00	1.00	1.00	1.00	1.00	1.13	1.37	1.52	1.89

Note: [$] shoshonite melt viscosity extrapolated (via a simple regression [$ln\ \eta$ (Pa s) = −7.09036 + 27695556/T^2] to low temperatures

η_r, relative viscosity; η_r(ER), relative viscosity calculated by Einstein-Roscoe equation with $\Phi_m = 0.6$.
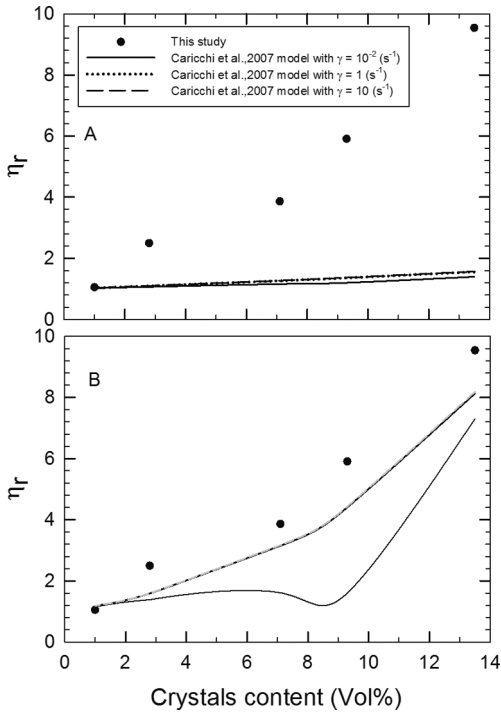
Figure 11. Comparison of the shoshonite relative viscosities with the viscosities calculated with the model described in Caricchi et al. (2007). Black circles represent the experimental data collected in this study. Lines were built with shear rates of 10^{-2}, 1, and 10 s^{-1} in (A) and (B). The differences in curvature result from the use of different values for the intrinsic viscosity parameter [e.g., in (A), $v = -2.5$; in (B), $v = -16.1$].

Figure 12. Relationship between relative viscosity, η_r, and crystal volume fraction, Φ. Black circles indicate the experimental data collected from this study. Data derived from the literature, from different literature models and from modified equations are shown as full, dashed, and dotted lines.

v see equation 1) of the modified equation (derived from the semi-empirical equation given by Costa et al., 2009) is equal to -2.5. The prediction obtained at the highest crystal content (e.g., $\Phi = 0.135$), yielded a relative viscosity value of $\eta_r < 2$ and was comparable to the value predicted by the ER equation (see Table 4). The experimental results yielded a $\eta_r = 9.5$ at high crystal contents (Fig. 11a). On the other hand, if the Caricchi et al. (2007) v parameter was increased to a value of -16.1 (which is reflective of the role played by the shape of the crystals), the modeled results were in better agreement with our experimental data obtained for shear rate ranges between 1 and 10 (Fig. 11b).

The marginally large relative viscosity observed for crystal contents of ~ 3 vol% in Figure 11 was somewhat odd. We conducted duplicate experiments to confirm the elevated viscosity values observed at low crystal contents. A similar elevation in the relative viscosity of suspensions with low crystal contents was reported by Yao and Matsumoto (1987). They ascribed the elevation in relative viscosity to interactions caused by elongated particles.

Mueller et al. (2010) gave a helpful overview on the rheology of partially crystallized systems. Experiments performed on analogical material give insight into the rheological properties of dilute, semi-dilute, and concentrated fields. According to that study, at very low particle volume fractions ($\Phi < 0.01$–0.02) the suspended particles are sufficiently well separated so that interactions between them are negligible. Rheology is Newtonian at low particle volume fractions and viscosity increases linearly with the particle volume fraction. At higher particle volume fractions ($0.01 < \Phi < 0.25$), probably due to hydrodynamic interactions among the particles, rheology is still Newtonian but the viscosity now increases considerably. This can be attributed to the increase of either prolate or oblate solids. At intermediate particle volume fractions, they found an excellent fit of the data using the Maron and Pierce equation (Maron and Pierce, 1956) that differs from the KD equation in regards to the exponential term, which in this case is equal to -2.

When we used the approach of Maron and Pierce (1956), the calculated value for η_r was not similar to the experimental results (best fit was obtained only with $\Phi_m = 0.20$; $R^2 = 0.86$). On the other hand, the KD equation with Φ_m and v as fitting parameters gave a better fit ($\Phi_m = 0.4$ and $v = 14.36$; $R^2 = 0.95$; see below and Fig. 12). Aspect ratios for the experiments performed at 1381 K showed that the S/I/L ratio of clinopyroxene was 0.11:0.16:1 whereas it was 0.14:0.94:1 for plagioclase (see the above discussion on the textural analyses). The average aspect ratio was ~ 7. These results could partially explain the abrupt increase in effective viscosity when the crystal content increased (Table 2 and Fig. 10).

Relative viscosity determinations

Relative viscosities, η_r, were calculated for each run temperature and are reported in Table 4 and Figures 12 and 13. Values for η_r increased monotonously with cooling-induced increases in the crystal fraction. The effect of crystals on the measured viscosities was evaluated by plotting the relative viscosity, η_r, against the volume fraction of the crystals, Φ. The relative viscosity increased consistently up to 9.5 for a volume fraction of crystals up to $\Phi = 0.135$.

As we already discussed, the ER equation is the equation most frequently used to predict the effects of crystals on relative viscosity. The ER equation is a version of the KD equation and is expressed as:

$$ln\ \eta_r = -v\ \Phi_m\ ln(1 - -\Phi/\Phi_m) \qquad (10),$$

where Φ is the crystal volume fraction and Φ_m is the maximum volume fraction of crystals. The ER equation represents the specific case where $v\ \Phi_m = 2.5$. In Figure 12, relative viscosities were calculated from equation (10) with varying values for v and Φ_m, and the results were compared with our experimental viscosity data. Figure 12 shows that it was difficult to explain our results by decreasing Φ_m at a constant v. Rather, large values of v (14-16) were required to explain our results using the KD equation. Because v is a parameter sensitive to the degree of interaction among crystals and hence, crystal shape, the value of v increases with the elongation of particles. In our experiments, we found evidence of elongated crystals (Fig. 3). Therefore, the whole system cannot be assumed to be a population of spheres.

In general, the η_r-Φ relationship can be represented by decreasing Φ_m when v is very high. However, it is important to point out that the relationship cannot be represented without a v value higher than that of the ER equation. Furthermore, decreasing Φ_m is not required when v is high i.e., increase of v is essential.

We used the least squares method to evaluate how well the KD equation fit our experimental data. We determined both the intrinsic viscosity and the maximum packing fraction simultaneously by least square fitting procedures. To complete this step, we used the following equation:

$$[\eta_r - (1 - \Phi/\Phi_m)^{-v\Phi m}]^2 \rightarrow min \qquad (11).$$

The best fit was obtained when intrinsic viscosity, v, was 14.36 and $\Phi_m = 0.4$ (Fig. 12; R^2 was 0.94). The KD equation seemed to reproduce the experimental data with good accuracy. However, a departure from the KD model

was observed when the crystal content increased to 13.5 vol%.

Recently, Vona et al. (2011) studied the behavior of partially crystallized basalts from the Stromboli and Etna volcanoes. They found a good agreement between their experimental data and data derived from a modified KD equation that used an adjustable α parameter ($\eta_r = (1 - \Phi/\Phi_m)^{-2[1-\alpha*\log(\gamma)]}$ where γ is the strain rate) to account for errors due to the Maron and Pierce approximation (e.g., $B\ \Phi_m = 2$). A non linear regression method was used with the equation described by Vona et al. (2011) to find the α coefficient in our analyses. This was done by changing the strain rate from 0.02 to 10. The results obtained were in good agreement with our experimental data only for α values of 0.95, 1.90, and -1.62 for which the strain rates varied from 0.02, 0.14, and 10, respectively. These results are shown in Figure 12 along with the modeled results obtained from the modified best fit KD equation (described above), the ER equation, and the equation presented in Sato (2005). In Figure 12, data obtained from Sato (2005), Ishibashi and Sato (2007), Ishibashi (2009), and Vona et al. (2011) are also reported.

The differences between the experimental data and the modeled data were interesting. The Ishibashi and Sato (2007) data were in good agreement with predictions obtained by the use of the ER equation, probably because of the lower aspect ratio of plagioclase (~ 4) and the presence of granular olivine, which can lead to a very different trend of feeble viscosity increase as a function of crystal content. Viscosity data from Vona et al. (2011) agreed well with the data obtained by Ishibashi (2009) for crystal contents up to 0.2. The similarity of these results was presumably due to the similar aspect ratios of the plagioclase crystals present in both studies. However, these results were different from the viscosity data obtained by Sato (2005) and by our present study. Comparable behaviors were observed for the Sato (2005) and the Ishibashi (2009) viscosity data on plagioclase-bearing basalts from a Fuji volcano, at plagioclase mean aspect ratios of 12.9 and 8.5, respectively. This comparable behavior amounted to an increase in relative viscosity as the crystal fraction increased. The strong increase in relative viscosity observed by Sato (2005) at very low crystal contents may be due to the very high aspect ratio of the plagioclase crystals in those experiments (see Fig. 12). Interestingly, in our experiments the plagioclase aspect ratio had an average value of 6.5 for the lowest temperature experiments (1381 K) but the measured viscosity was considerably higher than values presented in the literature (e.g., Vona et al., 2011: viscosity value of ~ 6000 Pa s at 1430 K for a partially crystallized Stromboli basalt with ~ 27 vol% of crystals; our results: viscosity value of ~ 15000 Pa s at

1381 K for ~ 14 vol% crystals). These discrepancies could be due to the relatively high elongated clinopyroxene crystals in our experiments (i.e., 9 vol% was represented by clinopyroxene crystals with $5 < AS \leq 16$; see Fig. 3a-1).

We would like to emphasize that the comparisons between our results and the literature values presented by Sato (2005), Ishibashi and Sato (2007), Ishibashi (2009), and Vona et al. (2011) were semi-quantitative and may have incurred errors when η_r was estimated (Fig. 12).

Data presented in Mueller et al. (2010) for relative consistency ($Kr = K/\mu_0$, where μ_0 is the viscosity of a liquid suspension and K is the consistency that can be considered as the parameter most closely related to the apparent viscosity; for a Newtonian suspension $K \equiv \eta$ and has the dimensions of viscosity, Pa s) are comparable with our experimental results because our systems behaved mostly as Newtonian fluids (discussed previously). Data obtained for prolate C particles (Table 1 in Mueller et al., 2010) have a mean $AS = 0.11$ and a relative consistency of 5.10 at $\Phi = 0.143$. The discrepancy between relative consistency and our relative viscosity at 1381 K (our data: $\Phi = 0.135$ and $\eta_r = 9.5$) is probably due to the fact that a portion of the crystals (~ 25 vol% and mainly plagioclase) have an AS higher than 10 (for a small numbers of crystals the maximum measured AS reaches a value of 20). Moreover, Mueller et al. (2010) did not use natural crystals and melts in their experiments. To simulate natural melts, Mueller et al. (2010) used silicone oil as a silicate melt analog, and art glitter, wollastonite, and angular silicone carbide grit as particles in the system.

A similar study was recently presented by Cimarelli et al. (2011), using a silicon oil as magma analog. Cimarelli et al. (2011) modeled viscosity behavior as the suspension varied in volume, shape, and size. In low particles concentration regions ($\Phi < 0.2$), they found that data derived from the Krieger and Dougherty (1959) approach were in good agreement with the experimental data. These results were also confirmed when the Costa et al. (2009) model was used. Different behavior is expected when particles exceed 20 vol%.

Simha (1940) proposed following equation for the determination of relative viscosities in the presence of rods-shaped crystals:

$$v = (\eta_r - 1)/\Phi$$
$$= f^2/[15*(log2f - 1.5)] + f^2/[5*(ln2f - 0.5)] + 14/15 \quad (12),$$

where f denotes the aspect ratio of the rod. Using this equation, we illustrated the possible effect of the rod's -shaped crystals aspect ratio on the relative viscosity
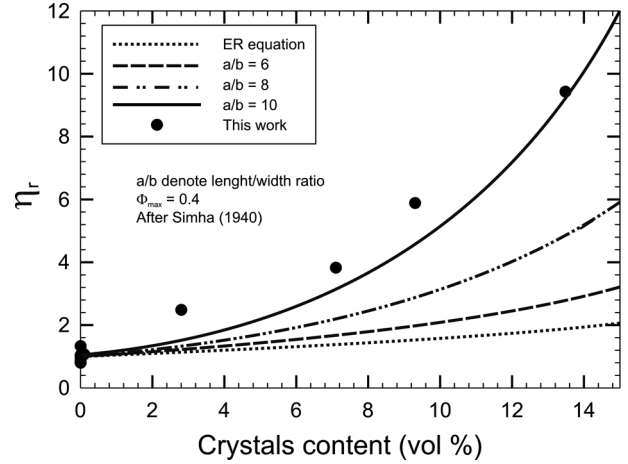

Figure 13. Relationship between relative viscosity, η_r, calculated after Simha (1940) and crystal content. Black circles indicate the experimental data collected from this study.

(Fig. 13). Results showed that the relative viscosity strongly increased as the aspect ratio of the rod-shaped crystals was changed from 6 to 8 to 10. These results demonstrate the enormous effect that a crystals elongation can have on magma rheology. Since high aspect ratios can cause large increases in relative viscosity, this may be an important mechanism that influenced the experimental results obtained from the Vulcanello sample in this study.

IMPLICATIONS FOR MAGMA EMPLACEMENT

Our results have implications for estimating instantaneous effusion rates in lava flows. At Vulcanello, the temperature during magma ascent and emplacement has been estimated to be ~ 1373 K (Zanon et al., 2003). Hence, we can use our effective viscosity data to estimate the lava flow velocity and effusion rate. The aspect ratio of crystals in natural rocks tends to be smaller than our experimental run products, so our estimate of the effusion rate may yield an upper limit.

Following Sakimoto and Gregg (2001), and considering that the surface velocity at z = 0 (z = cartesian coordinate; flow depth direction) is also the maximum velocity, u_{max}, one can calculate the maximum velocity of the lava flow in a location close to the emission fissure with the equation:

$$u_{max} = \frac{\rho \cdot g \cdot b^2 \cdot \sin(\theta)}{2 \cdot \eta} \quad (13),$$

where ρ, the density (kg m^{-3}); θ, the slope (°); η, the viscosity (Pa s); g, the gravity force (9.81 m s^{-2}); and b, the flow depth (m).

Table 5. Velocities and effusion rates calculated from the viscosity value obtained from concentric cylinder varying the slope

T (K)	B (m)	ρ Kg m^{-3}	g m s^{-2}	slope(°)	η Pa s	U_{max} m s^{-1}	Q/w m^3 s^{-1}
1381	1.5	2760	9.81	1	15320	0.015	0.035
1381	1.5	2760	9.81	5	15320	0.077	0.173
1391	1.5	2760	9.81	1	8201	0.029	0.065
1391	1.5	2760	9.81	5	8201	0.144	0.324

Note: B refers to the flow depth.

The instantaneous flow rate per unit width at the same location is given by:

$$\frac{Q}{w} = \frac{b^3 \cdot \rho \cdot g \cdot \sin(\theta)}{3 \cdot \eta} \tag{14},$$

where w is the flow width (m) and Q the flow rate (m^3 s^{-1}).

We can easily evaluate the instantaneous velocity and flow rate near the eruptive vent at Vulcanello by considering that: 1) the b value at Vulcanello is in the order of 1-2 *m* near the emission fissure; 2) the lava substratum is characterized by a nearly constant gentle slope (θ = 1-5°); 3) ρ_{DRE} = 2760 kg m^{-3} (considering a glass density of ~ 2650 kg m^{-3}, Vetere et al., 2007, and density for clinopyroxene of ~ 3200 kg m^{-3}); and 4) η derived from this study at the estimated effusive temperature of 1373 K is in the order of 10^4 Pa s. The results of this analysis are shown in Table 5. For a slope of 1°, lava velocities are in the order of ~ 0.02 m s^{-1} and increase to ~ 0.10 m s^{-1} when the slope approaches 5°, while Q is estimated to be 0.04 and 0.2 m^3 s^{-1}, respectively.

The primary difference between the Vulcanello platform lavas and our experimental products is the lack of groundmass crystals in our run products. This is due to the higher quenching rate experienced by the experimental melt with respect to that of lava flows. This feature may also explain the slightly higher phenocryst volume of lava flows with respect to our experimental run products.

The calculated instantaneous effusion rates were two orders of magnitude lower than the effusion rate calculated for Mount Etna (2.6-28.1 m^3 s^{-1}), and less than one order of magnitude lower than Kilauea (0.78-1.76 m^3 s^{-1}) and those measured for Stromboli lavas (0.55-0.85 m^3 s^{-1}) (Harris et al., 2007: data obtained from field-based instantaneous effusion rates and thermally derived time-averaged discharge rates). Moreover, it is interesting to note that a decrease in viscosity to a value of about 8200 Pa s (i.e., equivalent to a decrease in viscosity initiated by an increase in magmatic temperature from 1381 K to 1391K) caused an increase in velocity of ~ 0.015 m s^{-1} and 0.05 m s^{-1} when the slope varied from 1° to 5°, and an increase in the effusion rate of 0.03 m^3 s^{-1} and 0.14 m^3 s^{-1}, respective-

ly (Tables 2 and 5).

The Vulcanello flow rates are about one order of magnitude lower than those estimated for Mount Etna (15-45 m^3 s^{-1}), and the values are in agreement with the flow rates estimated at Hawaiian volcanoes in which the slopes are comparable, even though the viscosities are lower (up to 10^2 Pa s) than that of Vulcanello.

When compared with magmas of a similar degree of evolution but more silica undersaturated (e.g., phonotephrite of the 1944 lava flow at Mt. Vesuvius), the Vulcanello flow rate was one order of magnitude lower because of the lower viscosity of phonotephrite lavas, and possibly because of the higher alkali content (Mt. Vesuvius = 2.2 m^3 s^{-1} for a slope of 2° (Ventura and Vilardo, 2008).

CONCLUDING REMARKS

In summary, we investigated the effective viscosity of partially crystallized shoshonitic systems with low crystal contents (i.e., dilute dispersions). The shoshonitic magmas were obtained via cooling the shoshonite melt starting material from temperatures well above liquidus. Effective viscosities were then measured using concentric cylinder technique. We performed 10 viscosity measurements on systems containing only melts and on crystals-bearing systems with crystal contents up to 14 vol%. We observed a large increase in effective viscosity between 8 vol% and 14 vol% in our experiments, which can probably be attributed to crystals with relatively high aspect ratios. Our results showed a continuous increase in viscosity from 131 Pa s to 15320 Pa s as temperatures decreased. We conclude that the concentric cylinder technique is a valuable method to investigate magma rheology under naturally relevant conditions. However, the shear force imposed by the rod in the apparatus, which is insufficient to initiate movement at high crystal fractions, is a limitation.

Our study provides new data that may be used to constrain models for the emplacement of lava flows exhibiting Newtonian behavior, i.e., where flow velocity is inversely proportional to the viscosity of the crystal-melt suspension, and the heat released from viscous dissipation is proportional to the viscosity (Harris and Rowland,

2001). Alignment of crystals was not obvious in our experiment, although elongated pyroxene crystals were observed, and their interaction most likely caused the elevated relative viscosities observed in this experiment. A variety of different models were used to fit the experimental data. Analyses of these models indicate that a high ν value is required to have good predictive capabilities for estimating the relative viscosity of partially crystallized shoshonite. These findings are likely due to the large impact that elongated crystals can have on magma rheology.

ACKNOWLEDGMENTS

REFERENCES

Arbaret, L., Bystrycky, M. and Champallier, R. (2007) Microstructures and rheology of hydrous synthetic magmatic suspensions deformed in torsion at high pressure. Journal of Geophysical Research, 112, B10208, 1-24.

Arrighi, S., Tanguy, J.C. and Rosi, M. (2006) Eruptions of the last 2200 years at Vulcano and Vulcanello (Aeolian Islands, Italy) dated by high-accuracy archeomagnetism. Physics of Earth and Planetary Interior, 159, 225-233.

Blanco-Montenegro, I., De Ritis, R. and Chiappini, M. (2007) Imaging and modelling the subsurface structure of volcanic calderas with high resolution aeromagnetic data at Vulcano (Aeolian Islands, Italy). Bulletin of Volcanology, 69, 643-659.

Caricchi, L., Burlini, L., Ulmer, P., Gerya, T., Vassalli, M. and Papale, P. (2007) Non-Newtonian rheology of crystal-bearing magmas and implications for magma ascent dynamics. Earth and Planetary Science Letters, 264, 402-419.

Caricchi, L., Diordano, D., Burlini, L., Ulmer, P. and Romano, C. (2008) Rheological properties of magma from the 1538 eruption of Monte Nuovo (Phlegrean Fields, Italy): An experimental study. Chemical Geology, 256, 158-171.

Champallier, R., Bystrichy, M. and Arbaret, L. (2008) Experimental investigation of magma rheology at 300 Mpa: from pure hydrous melt to 76 vol.% of crystals. Earth and Planetary Science Letters 263, 571-583.

Cimarelli, C., Costa, A., Mueller, S. and Mader, H.M. (2011) Rheology of magmas with bimodal crystals size and shape distributions: insights from analog experiments. Geochemistry, Geophysics, Geosystems, 12, Q07024, doi:10.1029/2011GC 003606.

Cordonnier, B. Hess, K.-U., Lavallee, Y. and Dingwell, D.B. (2009) Rheological properties of dome lavas: Case study of Unzen volcano. Earth and Planetary Science Letters, 279, 263-272.

Costa, A. (2005) Viscosity of high crystal content melts: dependence on solid reaction. Geophysical Research Letters, 32, L22308, 1-5.

Costa, A., Caricchi, L. and Bagdassarov, N. (2009) A model for the rheology of particle-bearing suspensions and partially molten rocks. Geochemistry, Geophysics, Geosystems, doi:10.1029/2008GC002138.

Cox, M.R. and Budhu, B. (2008) A practical approach to grain shape quantification. Engineering Geology, 96, 1-16.

Davì, M., De Rosa, R., Donato, P., Vetere, F., Barca, D. and Cavallo, A. (2009) Magmatic evolution and plumbing system of ring-fault volcanism: the Vulcanello Peninsula (Aeolian Islands, Italy) European Journal of Mineralogy, 21, 1009-1028.

De Astis, G., Dellino, P., La Volpe, L., Lucchi, F. and Tranne, C.A. (2006) Geological map of the Vulcano Island. Litografia 95 artistica cartografica, Firenze.

Dellino, P. and La Volpe, L. (1996) Image processing analysis in reconstructing fragmentation and transportation mechanisms of pyroclastic deposits. The case of Monte Pilato-Rocche Rosse eruptions, Lipari (Aeolian islands, Italy). Journal of Volcanology and Geothermal Research, 71, 13-29.

Dingwell, D.B. (1991) Redox viscometry of some Fe-bearing silicate melts. American Mineralogist, 76, 1560-1562.

Dingwell, D.B. and Virgo, D. (1988) Viscosity oxidation state relationship for hedenbergitic melt. Carnegie Inst. Wash. Yearbook, 87, 48-53.

Einstein, A. (1906) Eine neue Bestimmung der Molekuldimensionen. Annals of Physics, 19, 289-306.

Gioncada, A., Clocchiatti, R., Sbrana, A., Bottazzi, P., Massare, D. and Ottolini, L. (1998) A study of melt inclusions at Vulcano (Aeolian Islands, Italy): insights on the primitive magmas and on the volcanic feeling system. Bulletin of Volcanology, 60, 286-306.

Giordano, D., Russel, K.J. and Dingwell, D.B. (2008) Viscosity of magmatic liquids: a model. Earth and Planetary Science Letters, 271, 123-134.

Harris, A.J.L. and Rowland, S.K. (2001) FLOWGO: a kinematic thermo-rheological model for lava flowing in a channel. Bulletin of Volcanology 63, 20-44.

Harris, A.J.L., Dehn, J. and Calvari, S. (2007) Lava effusion rate definition and measurement: a review. Bulletin of Volcanology, 70, 1-22.

Higgings, M.D. (2000) Measurement of Crystal Size Distributions. American Mineralogist, 85, 1105-1116.

Huebner, J.S. (1982) Use of gas mixtures at low pressure to specify oxygen and other fugacities of furnace atmospheres. In Hydrothermal Experimental Techniques (Ulmer, G.C. and Barnes, H.L. Eds.). John Wiley & Sons, NewYork, 20-60.

Krieger, I.M. and Dougherty, T.J. (1959) A mechanism for non-Newtonian flow in suspensions of rigid spheres. Transactions of the Society of Rheology, 3, 137-152.

Iezzi, G. and Ventura, G. (2002) Crystal fabric evolution in lava flows: results from numerical simulations. Earth and Planetary Science Letters, 200, 33-46.

Ishibashi, H. (2009) Non-Newtonian behavior of plagioclase-bearing basaltic magma: subliquidus viscosity measurement of the 1707 basalt of Fuji volcano, Japan. Journal of Volcanology and Geothermal Research, 181, 78-88.

Ishibashi, H. and Sato, H. (2007) Viscosity measurements of subliquidus magmas: alkali olivine basalt from the Higashi-Matsuura district, Southwest Japan. Journal of Volcanology and Geothermal Research, 160, 223-238.

Krieger, I.M. and Dougherty, T.J. (1959) A mechanism for non-Newtonian flow in suspensions of rigid spheres. Transaction of the Society of Rheology, 3, 137-152.

Landau, L.D. and Lifschitz, E.M. (1970) Fluid Mechanics (Japanese edition translated by Takeuchi, H.). Tokyu-Gakujutsu Tosho, Co. Ltd. (translated in Japanese).

Lejeune, A.M. and Richet, P. (1995) Rheology of crystal-bearing silicate melts- an experimental study at high viscosities. Journal of Geophysical Research: Solid Earth, 100, 4215-4229.

Le Maitre, R.W. (1979) A new generalized petrological mixing model. Contributions to Mineralogy and Petrology, 71, 133-137.

Liebske, C., Behrens, H., Holtz, F. and Lange, R.A. (2003) The influence of pressure and composition on the viscosity of andesitic melts. Geochimica et Cosmochimica Acta, 67, 473-485.

Loncaric, S. (1998) A survey of shape analysis techniques. Pattern Recognition, 31, 983-1001.

Maron, S.H. and Pierce, P.E. (1956) Application of Ree-Eyring generalized flow theory to suspensions of spherical particles. Journal of Colloid Science, 11, 80-95. (doi:10.1016/0095-8522(56)90023-X)

Marsh, B.D. (1981) On the crystallinity, probably occurrence, and rheology of lava and magma. Contributions to Mineralogy and Petrology 78, 85-98.

Mueller, S., Llewellin, E.W. and Mader, H.M. (2010) The rheology of suspensions of solid particles. Proceedings of the Royal Society, A, 466, 1201-1228. DOI: 10.1098/rspa.2009.0445

Murase, T. and McBirney, A.R. (1973) Properties of some common igneous rocks and their melts at high temperatures. Geological Society of America Bulletin, 84, 3563-3592.

Murase, T., McBirney, A.R. and Melson, W.G. (1985) Viscosity of the dome of Mount St. Helens. Journal of Volcanology and Geothermal Research, 24, 193-204.

Mysen, B.O. and Virgo, D. (1989) Redox equilibria, structure and properties of Fe-bearing alumosilicate melts: relationship among temperature, composition and oxygen fugacity in the system $Na_2O-Al_2O_3-SiO_2-Fe-O$. American Mineralogist, 74, 58-76.

Peccerillo, A., Frezzotti, M.L., De Astis, G. and Ventura, G. (2006) Modeling the magma plumbing system of Vulcano (Aeolian Islands, Italy) by integrated fluid-inclusion geobarometry, petrology and geophysics. Geology, 34, 17-20.

Pinkerton, H. and Stevenson, R.J. (1992) Methods of determining the rheological properties of magmas at suliquidus temperature. Journal of Volcanology and Geothermal Research, 53, 47-66.

Pinkerton, H. and Norton, G. (1995) Rheological properties of basaltic lavas at sub-liquidus temperatures: laboratory and field measurements on lavas from Mount Etna. Journal of Volcanology and Geothermal Research, 68, 307-323.

Roscoe, R. (1952) The viscosity of suspensions of rigid spheres. British Journal of Applied Physics, 3, 267-269.

Ryerson, F.J., Weed, H.C. and Piwinskii, A.J. (1988) Rheology of subliquidus magmas 1. Picritic compositions. Journal of Geophysical Research, 93, 3421-3436.

Sakimoto, S.E.H. and Gregg, T.K.P. (2001) Channeled flow: ana-lytic solution, laboratory experiments and application to lava flows. Journal of Geophysical Research, 106, 8629-8644.

Sato, H. (2005) Viscosity measurements of subliquidus magmas: 1707 basalt of Fuji volcano. Journal Mineralogy and Petrology Sciences, 100, 133-142.

Shaw, H.R. (1969) Viscosity of basalt in the melting range. Journal of Petrology, 10, 510-535.

Shaw, H.R. (1972) Viscosities of magmatic silicate liquids: an empirical method of prediction. American Journal of Science, 272, 870-893.

Simha, R. (1940) The influence of Brownian movement on the viscosity of solutions. Journal of Physical Chemistry. 44, 25-34.

Spera, F.J., Borgia, A. and Strimple, J. (1988) Rheology of melts and magmatic suspensions, Design and calibration of concentric cylinder viscometer with application to rhyolitic magma. Journal of Geophysical Research, 93, 10273-10294.

Ventura, G., Vilardo, G., Milano, G. and Pino, N.A. (1999) Relationship among crustal structure, volcanism and strike-slip tectonics in the Lipari-Vulcano Volcanic Complex (Aeolian Islands, Southern Tyrrhenian Sea, Italy). Physics of the. Earth and Planetary Interior, 116, 31-52.

Ventura, G. and Vilardo, G. (2008) High resolution Lidar data provide insights into the emplacement mechanism of gravity flows: a case study from the 1944 Somma-Vesuvius lava flow (Italy). Geomorphology, 95 223-235.

Vetere, F., Behrens, H., Misiti, V., Ventura, G., Holtz, F., De Rosa, R. and Deubner, J. (2007) The viscosity of shoshonitic melts (Vulcanello Peninsula, Aeolian Islands, Italy): Insight on the magma ascent in dikes. Chemical Geology, 245, 89-102.

Vetere, F., Behrens, H., Schuessler, J., Holtz, F., Misiti V. and Borchers, L. (2008) Viscosity of andesite melts and its implication for magma mixing prior to Unzen 1991 - 1995 eruption. Journal of Volcanology and Geothermal Research, 175, 208-217. Doi: 10.1016/j.jvolgeores. 2008.03.028

Vetere, F., Behrens, H., Holtz, F., Vilardo, G. and Ventura, G. (2010) Viscosity of crystal-bearing hydrous andesites and its implication for magma ascent. Journal of Mineralogical and Petrological Sciences, 105, 151-163.

Vona, A., Romano, C., Dingwell, D.B. and Giordano, D. (2011) The rheology of crystals-bearing basaltic magmas from Stromboli and Etna. Geochimica et Cosmochimica Acta, 75, 3214-3236.

Yao, S. and Matsumoto, T. (1987) New type of equation for the relation between viscosity and particle content in suspensions. Journal of Non-Newtonian Fluid Mechanics, 25, 197-207.

Zanon, V., Frezzotti, M.L. and Peccerillo, A. (2003) Magmatic feeding system and crustal magma accumulation beneath Vulcano Island (Italy): evidence from fluid inclusions in quartz xenoliths. Journal of Geophysical Research, 108, 1-13.